RAL-TR-2004-022

The Use of Fluorinated Mica as a Crystal Analyser on IRIS

Mark A. Adams[1]

and

F Fernandez-Alonso[1], D T Maxwell[1], J Vine[1],
D D Abbley[1], J Stahn[2]

1. ISIS Facility, CCLRC, RAL

2. LNS, SINQ, Paul Scherrer Institute, Villigen-PSI, Switzerland

Abstract

The potential use of a synthetic fluorinated mica, fluorophlogopite, as an analyser crystal on the high resolution inelastic neutron scattering spectrometer IRIS has been investigated. In-situ measurements on IRIS and single crystal diffraction measurements at the Paul Scherrer Institute in Switzerland have been made in order to characterise this material.

A direct comparison with the muscovite mica currently in use on IRIS shows that the fluorophlogopite is superior both in terms of reflected intensity and signal-background.

Acknowledgement

Many thanks to Prof. John Larese, University of Tennessee, Oak Ridge, U.S.A. for the supply of the fluorophlogopite used in this study and also to Dr. Colin Carlile, Director, ILL for the original suggestion that fluorinated mica would be a better choice than natural mica for a crystal analyser material.

IRIS

IRIS [1] [2] is the highest resolution inelastic neutron scattering spectrometer at the pulsed spallation neutron source, ISIS [3]. It is a crystal analyser spectrometer in which neutrons with a range of wavelengths are incident on the sample position and the scattered neutrons are energy-analysed by being Bragg reflected from single crystals. For the purpose of description the spectrometer can be divided into two sections: a primary spectrometer consisting of a ~36.5m long flightpath over which the neutron pulses generated by two neutron disk choppers disperse, providing the time component of the resolution function and the secondary spectrometer (fig. 1) containing the crystal analyser banks and the detectors.

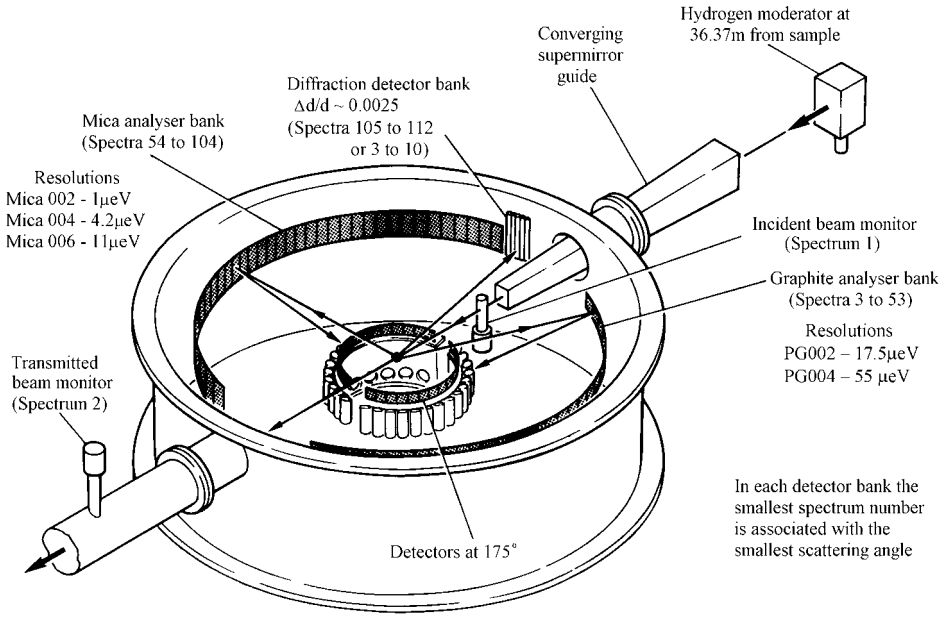

Figure 1. The IRIS Secondary Spectrometer

One of the strengths of the instrument is the flexibility introduced by the use of two types of crystal analyser bank – pyrolytic graphite and the natural mica material, muscovite. This makes it possible to select from a number of different combinations of energy resolution, energy-transfer window, Q-resolution and Q-range. The more usual options are shown in table 1.

Clearly, although the mica analyser options provide for much improved resolution and access to lower Q-values they suffer from a lack of intensity due to an inherently lower incident flux of long wavelength neutrons and lower reflectivities for the mica reflections c.f. the graphite reflections.

Table 1. Standard Inelastic Settings on IRIS for the pyrolytic graphite (PG) and mica (M) reflections

Analyser reflection and Intensity relative to PG002	Resolution (FWHM) at elastic line (μeV)	Chopper operating frequency	ΔE (meV)	$\Delta Q_{elastic}$ (Å^{-1})
PG004 (0.7)	55.0	50	-3.5 to 4.0	0.844 to 3.719
PG002 (1.0)	17.5	50	-0.4 to 0.4	0.422 to 1.859
PG002 (1.0)	17.5	50	-0.2 to 1.2	0.422 to 1.859
PG002 (0.5)	17.5	25	-0.8 to 0.8	0.422 to 1.859
PG002 (0.33)	17.5	16.7	-1.0 to 10.0	0.422 to 1.859
M006 (0.4)	11.0	50	-0.4 to 0.4	0.396 to 1.864
M004 (0.15)	4.5	50	-0.15 to 0.15	0.264 to 1.263
M002 (0.04)	1.2	50	-0.02 to 0.02	0.132 to 0.621

However, this is not the biggest drawback in using the mica analyser bank. It is the very poor signal-background (~ 80:1 for the (002) reflection) which restricts the use of this analyser to quasielastic scattering from strongly scattering i.e. hydrogenous systems. As mentioned previously this is in part due to the low reflectivities for this material but also, perhaps more importantly, it is associated with the presence of OH^- ions within this naturally occurring mineral. The large neutron incoherent scattering cross-section of the proton (~ 80 barns, some 20 times larger than most other elements) leads to a large background at all neutron wavelengths. In comparison, the PG analyser, for which the neutron reflectivity is higher and the incoherent scattering cross-section very low (0.001 barns), exhibits a signal-background of some 3500:1 (after the introduction of cooling to reduce the effect of thermal diffuse scattering [1,4]).

Clearly, a hydrogen-free analyser crystal would be of interest but in order not to have to re-design the instrument totally it should be very similar to muscovite mica i.e. a similar d-spacing mica crystal but without the protons.

The Micas[5-8]

Mica is a generic term referring to a group of minerals which are members of the subclass of silicates called phyllosilicates which form sheet-like structures consisting of rings of tetrahedrons linked by shared oxygen atoms to other rings of tetrahedrons. Typically, the sheets are then connected to each other by layers of cations which are weakly bonded and often have water molecules and other neutral atoms or molecules trapped between the sheets.

In the micas (fig. 2) interlinked six-membered rings of SiO_4 tetrahedra form sheet structures consisting of two tetrahedral layers with an octahedral layer containing small ions such as aluminium in between. These tetrahedral–octahedral–tetrahedral layers (TOT) are then separated by a cation interlayer .

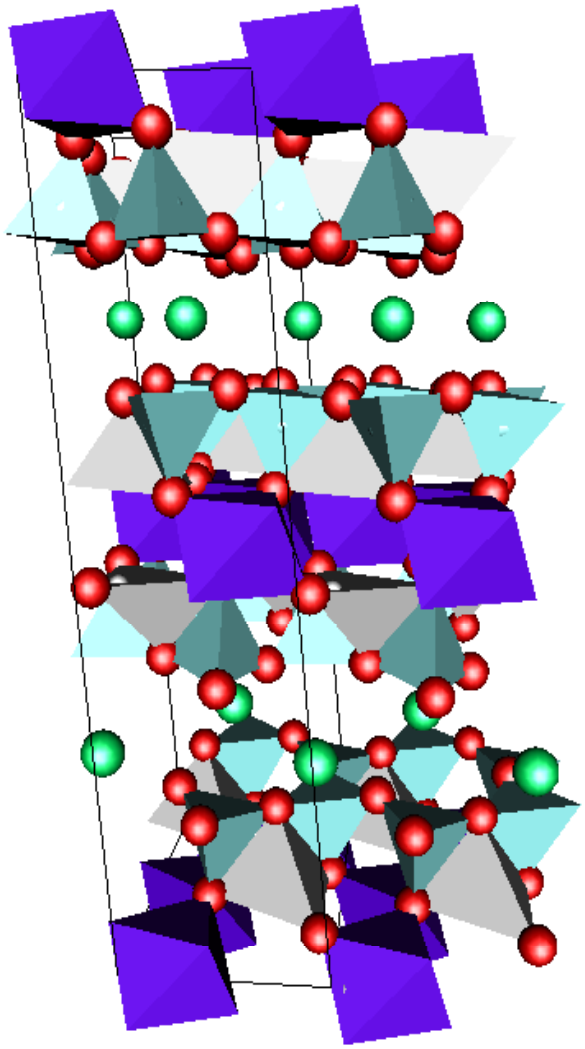

Figure 2. Generic mica structure

The general formula for the micas is $AB_{2-3}(X, Si)_4O_{10}(O, F, OH)_2$. In most micas the A ion is usually potassium but can also be sodium, calcium, barium, caesium and/or ammonium. These ions occupy positions in the cation interlayer. The B ion can be either aluminium, lithium, iron, zinc, chromium, vanadium, titanium, manganese and/or magnesium. These ions occupy positions in the octahedral layers of the TOT. The X ion is usually aluminium but can also be beryllium, boron and/or iron and they sit in the centre of the tetrahedrons substituting for silicons by up to 50%.

Fluorophlogopite

Unfortunately, all natural micas which are suitable for use as monochromating devices, contain OH^- ions. However a synthetic, fluorinated, version of the natural mica, phlogopite (Potassium magnesium aluminium silicate hydroxide - $KMg_3(AlSi_3O_{10})(F,OH)_2$), can be obtained commercially. In fluorophlogopite all the OH^- ions have been replaced by F^- ions to give $KMg_3(AlSi_3O_{10})F_2$. Fluorine, like carbon, has a very low incoherent scattering cross-section (0.0008 barns) and so fluorophlogopite should have a much reduced background from incoherent scattering.

Large fluorophlogopite crystals of high quality are grown by a Bridgman-Stockbarger method using platinum crucibles with seed crystals. It is more easily cleavable than the natural variant and is suitable for use as windows and monochromators for x-ray and neutron diffraction.

The crystallographic parameters for muscovite and fluorophlogopite are shown in Table 2. This indicates that the two materials are similar enough to be inter-changeable.

Table 2. Crystallographic comparison of Muscovite and Fluorophlogopite

	a (Å)	B (Å)	c (Å)	β °	Z	V (Å^3)	ρ (gcm^{-3})*
Muscovite	5.19	9.03	20.05	95.5	4	935.33	2.83
Fluorophlogopite	5.31	9.183	20.278	100.07	4	973.56	2.87

* Calculated density

Incoherent Background

An idea of the expected reduction in incoherent scattering background can be gained by a simple comparison of the neutron scattering cross-sections of the two micas, muscovite and fluorophlogopite (Table 3).

The incoherent scattering background scales as the number density, N, the incoherent scattering cross-section, σ_i and the thickness, t. For the two materials N is very similar (muscovite - 4.274×10^{21}, fluorophlogopite – 4.1085×10^{21}) so assuming identical thicknesses the expected reduction in background due to incoherent neutron scattering scales with the incoherent cross-section and is considerable (~ 300). However, apart from the issue of

incoherent scattering background there are other factors to be considered when determining the likely improvement in signal-background and hence the usefulness of this particular mica as an analyser crystal on IRIS.

Table 3. Comparison of neutron cross-sections per formula unit

MICA (Empirical Formula)	Total σ_i (barns)	Total σ_c (barns)	Total σ_a (barns)
Muscovite $KAl_3Si_3O_{10}(OH)_2$	160.82	66.96	3.99
Fluorophlogopite $KMg_3AlSi_3O_{10}F_2$	0.53	70.92	3.07

	Neutron cross-sections (barns)		
Element	Coherent	Incoherent	Absorption
K	1.69	0.27	2.1
Mg	3.631	0.08	0.063
Al	1.495	0.0082	0.231
Si	2.163	0	0.177
O	4.232	0.0008	0.00019
H	1.7568	80.26	0.3326
F	4.017	0.0008	0.0096

Structure factors and attenuation

Clearly, a major influence on the performance of fluorophlogopite, both in terms of intensity and signal-background, is the structure factor for the various reflections which would be used on IRIS. However, another equally important characteristic, is the presence of neutron beam attenuation due to extinction, absorption and, again, incoherent scattering. It is known that primary extinction is not usually a problem in typical mosaic crystals but secondary extinction may play a role in reducing the reflected intensity below that expected from structure factor considerations alone. Determining the effect of secondary extinction is not straightforward and it is usually treated as a set of refineable parameters from a measured diffraction pattern (see Appendix A). For the moment, therefore, we shall concentrate on the other attenuating factors.

The reflection and attenuation characteristics of muscovite and fluorophlogopite have been calculated using nominal structures for these micas and tabulated cross-section data [9]. A summary of the results is shown

in Table 4. This indicates that for the same thickness of material and at a similar wavelength to that used on IRIS the peak reflectivity of the (002)

Table 4. Calculated attenuation factors and peak reflectivities for fluorophlogopite and muscovite

		Fluorophlogopite		Muscovite	
λ (Å)		1.9	17.4	1.9	17.4
Attenuation Factors	Incoherent (cm^{-1})	0.002	0.002	0.688	0.688
	Absorption (cm^{-1})	0.013	0.116	0.018	0.186
	Total (cm^{-1})	0.015	0.118	0.706	0.874
FWHM (^{o})		0.3	0.3	0.2	0.2
Peak Reflectivity (0.25mm Thick Crystals)		0.11	**0.69**	0.030	**0.037**

reflection in fluorophlogpite (λ~20 Å) is expected to be almost 20 times that of muscovite. Furthermore, it is clear that not only is the incoherent scattering cross-section in muscovite a major source of background but it is also a significant attenuating factor. This will impact greatly on any attempt to increase reflected intensity by increasing the thickness of the crystals. It is notable that originally the muscovite mica analyser bank on IRIS consisted of 0.25mm thick crystals stacked to a thickness of 4mm. This overall thickness was reduced to 1mm with no discernible effect on the reflected Bragg intensity indicating that the reflected intensity had already saturated at 1mm thickness. In the case of fluorophlogopite, attenuation due to incoherent scattering is almost negligible and it has been proposed that fluorophlogopite crystals can be stacked to thicknesses of more than a centimetre to increase the neutron reflectivity [9]. It is important to test this proposition.

In-situ Comparison of Muscovite and Fluorophlogopite Micas

Obviously, a very direct method of assessing the effect of replacing muscovite with fluorophlogopite is to just do it and make an in-situ comparison. A free source of fluorophlogopite became available and this is what was done.

The IRIS mica analyser bank (figs. 3 and 4) consist of a support stand upon which 23 individual backing plates sit. Each of these plates (which are curved to provide the necessary focussing effect – fig. 5) has six positions available for the mica crystals. The original muscovite mica crystals are 100 x 30 x 0.25 mm and 4 of these are stacked together at each position giving a millimetre thickness throughout. The crystals are held on to the support blocks by a screw through the centre which is covered by a piece of neutron absorbing cadmium to reduce background.

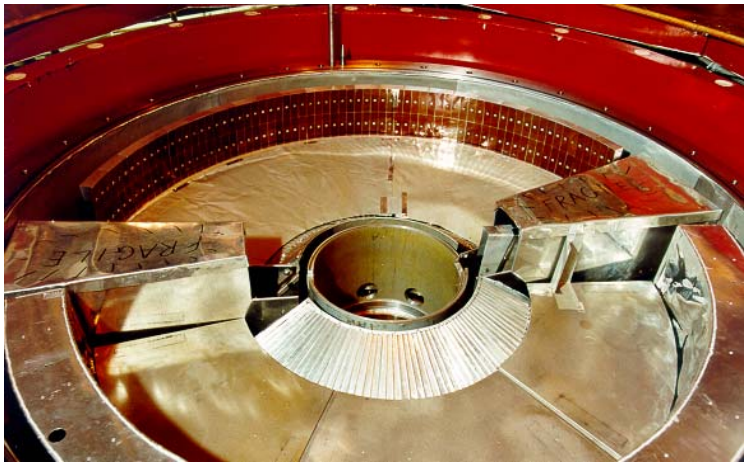

Figure. 3 The IRIS analyser tank with the muscovite analyser at the back

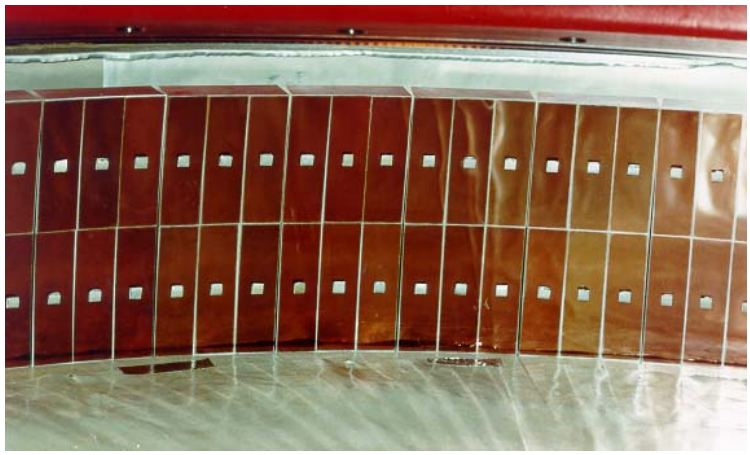

Figure. 4 Close-up of the muscovite mica analyser bank

Figure. 5 The curved profile of the mica backing plates

The fluorophlogopite crystals are nominally (see later) 75 x 25 x 0.1 mm and figure 6 shows them at the half-way stage of installation (bottom row positions only). It is important to note the reduction in surface area covered by this mica and the fact that we are going to be comparing 0.1 mm thick fluorophlogopite with the 1mm thickness of the original muscovite.

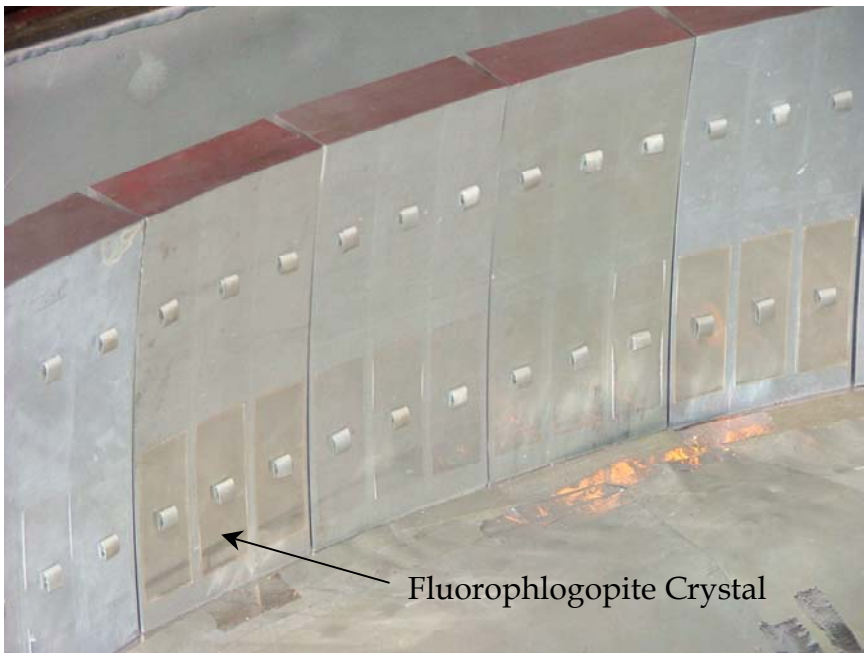

Figure 6. The installation of fluorophlogopite at the half-way stage

For the first test in which a single crystal was placed at each of the 138 positions it was assumed that the thickness was as quoted, i.e. 0.1mm. However, it was later discovered that there was a distribution of thicknesses. Each individual piece was therefore measured and the distribution of thicknesses is shown in figure 7.

A statistical analysis show that average thickness for the 154 crystals is 0.1082 ± 0.0215 mm. None of the very thin crystals were used in the first test (some of the crystals were noticeably more flexible) and this yields an average thickness for this measurement of 0.1124 ± 0.0184 mm and so a value of 0.11mm for the average thickness will be assumed from now on.

In order to properly assess the effect of changing the analyser crystals an instrument calibration must be carried out. Usually this is done with a standard sample of vanadium (3 concentric cylinders of 0.04mm thick vanadium foil with diameters of 10, 16 and 20mm) which is a purely elastic incoherent scatterer over the energy-transfer range available on IRIS. Unfortunately for the longer wavelength mica (002) setting this is not appropriate. Vanadium has a 5 barn absorption cross-section and although it is only a 0.7% absorber at 6.7Å the non-isotropic scattering this introduces becomes much more apparent at longer wavelengths (~2% absorber at 20Å). An alternative standard sample has therefore been produced by wrapping a

0.1mm thick sheet of polyethylene inside a standard IRIS aluminium alloy annular geometry can with an external diameter of 20mm. In figures 8 and 9 the measured resolution functions or "elastic lines" of the instrument are shown for the muscovite and fluorophlogopite analyser configurations.

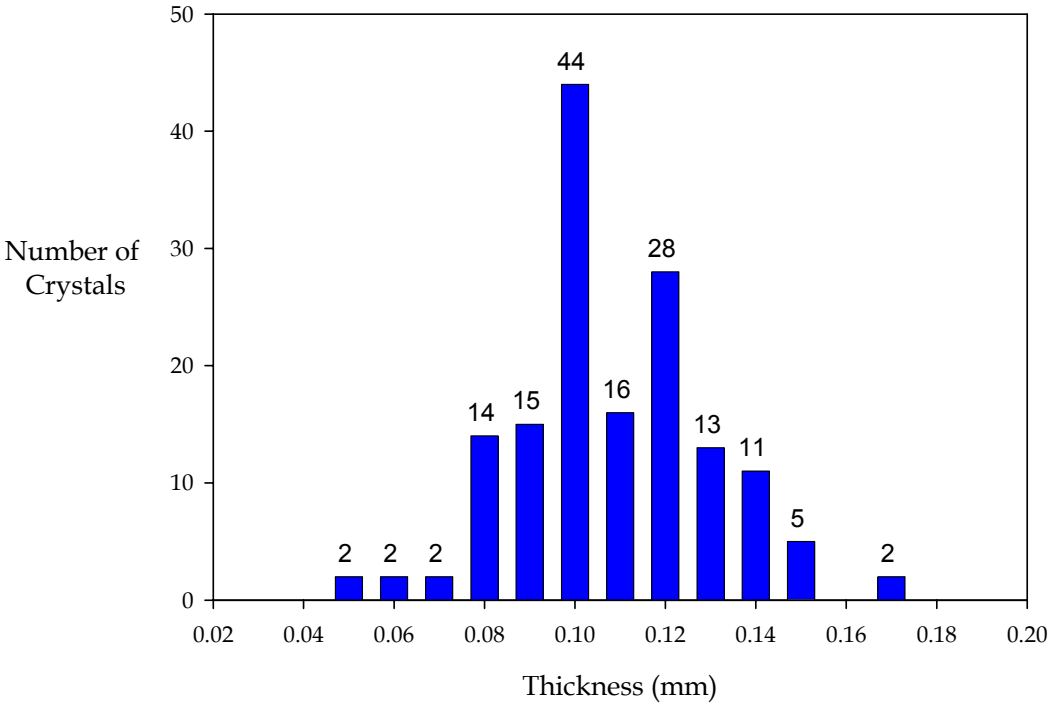

Figure. 7 Distribution of thicknesses for the fluorophlogopite crystals

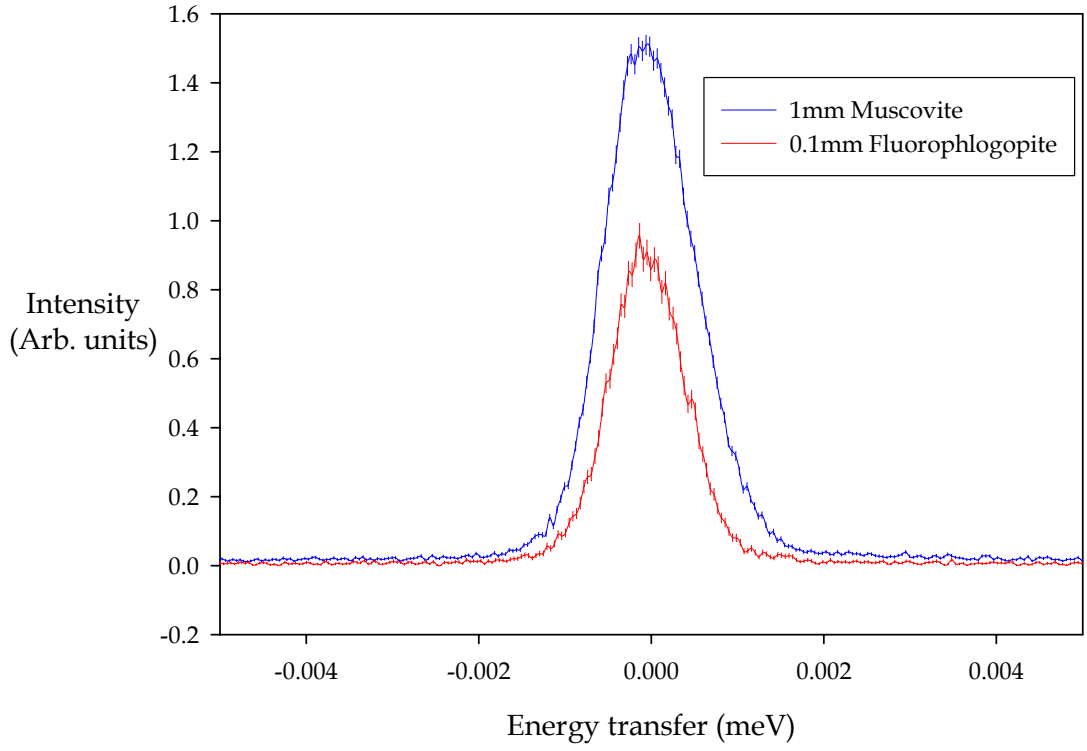

Figure 8. Elastic line comparison for muscovite and fluorophlogopite

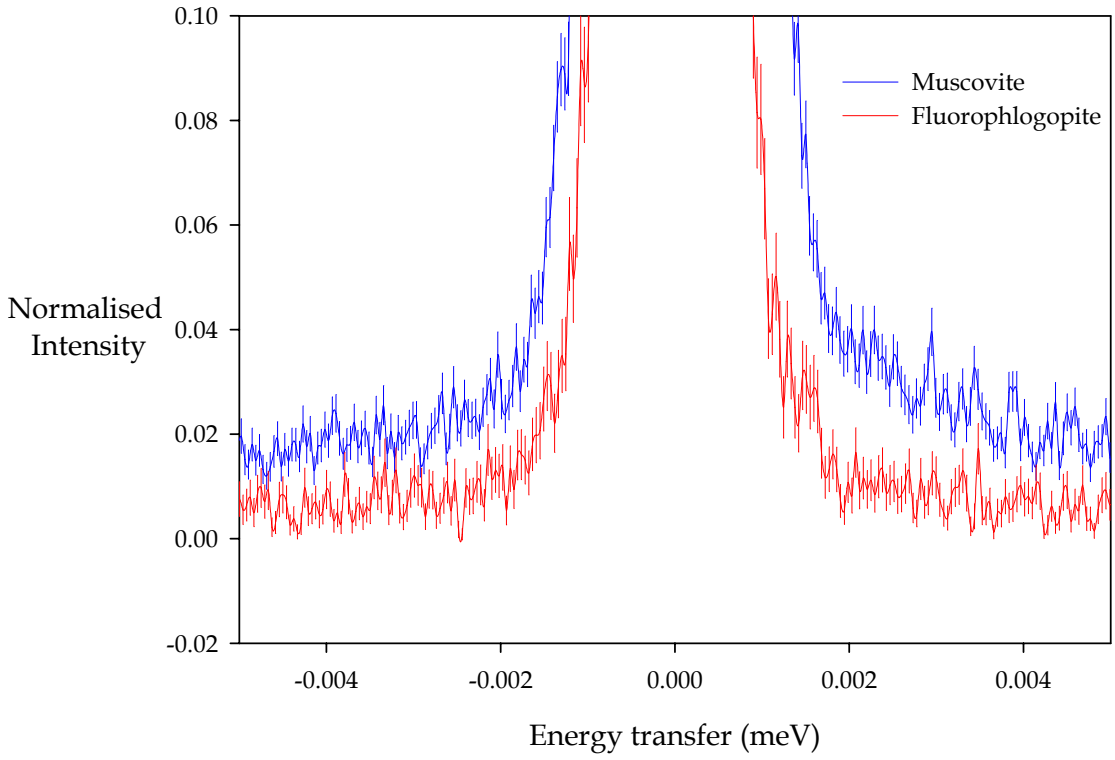

Figure 9. Background level comparison for muscovite and fluorophlogopite

The peaks were fitted with Gaussian functions of the form:

$$y = y_0 + a_0 \exp\left[-\frac{1}{2}\left(\frac{x - a_1}{a_2}\right)^2\right] \qquad (1)$$

where y_0 is a background offset, a_0 is the amplitude, a_1 is the centre of the Gaussian and a_2 is the width parameter corresponding to the standard deviation,σ. In order to extract the resolution width we use the fact that the full width at half maximum of a Gaussian function is $2.35482 \times \sigma$. Table 5 shows the extracted parameters for the fits.

The signal-background can be defined in a number of different ways. For the purposes of this comparison it's not essential which way is chosen as long it is consistent throughout. With reference to the Gaussian fitting equation we shall define the signal-background ratio using:

$$S/B = \frac{a_0 - y_0}{y_0} \qquad (2)$$

Table 5. Extracted resolution parameters for muscovite and fluorophlogopite

	Muscovite	Fluorophlogopite
Energy Resolution ΔE (μeV)	1.23	1.03
Peak amplitude a_0	1.4911	0.8991
Signal-background	79.3	136.1

It's clear from the data in the table that the expected dramatic improvement in signal-background has not taken place which probably indicates the presence of other sources of background. This will be investigated at a later date. However, an improvement in signal-background of ~70% is still worthwhile having and in addition the resolution has improved. But, as mentioned previously, the most important factor to be tested is the potentially huge increase in intensity available by increasing the thickness of the fluoroplogopite. In these measurements the intensity of the (002) reflection in fluorophlogopite is less than that from the muscovite but it must be remembered that we are not comparing like with like. The first factor to be considered is the relative area of the two analyser set-ups which is (100 x 30)/(75 x 25) = 1.6. Just using this factor a drop in intensity of 0.62 is expected and this is almost exactly what is observed (actually 0.60). Secondly, and more importantly, we are comparing 0.11mm thick fluorophlogite with 1mm thick muscovite. This indicates that from this data for the same thickness of material (1mm) we should expect an increase of a factor of 9 in the intensity of the (002) reflection in going from muscovite to fluorophlogopite. This does not agree with the structure factor calculations where a factor of 20 was suggested. It is clear therefore that it is very important to investigate the effect of thickness on the reflectivity of fluorophlogopite.

The effect of thickness on the reflected intensity from fluorophlogopite

A second experiment was carried out on IRIS in which the thickness of fluorophlogopite at different positions on the analyser bank was varied. The aim was to have a range of thicknesses from 0.1 up to 1.2mm spread over the analyser bank. The placement of the 154 fluorophlogopite crystals followed the schema detailed in Tables 6 and 7. In table 6 the '3' refers to three single mica crystals, one at each of the three crystal positions on the bottom row of a support block. Similarly, '[A1,A2,A3]' implies the sequential installation of configurations A1, A2, and A3. Other configurations are labelled 'B', 'C', etc. and follow the same logic. The meaning of these labels is shown in table 7.

In order to normalise the data it was decided to assume that the original muscovite mica scattered equally well at all angles and therefore any variation in detected flux is purely as a result of differences in detection efficiency. Therefore a run taken with mica 002 standard settings using the

Table 6. Mica analyser bank positions

1	2	3	4	5	6	7	8	9	10	11	12	13	14	15	16	17	18	19	20	21	22	23
0	0	0	0	0	0	0	0	0	0	0	0	0	0	0	0	0	0	0	0	0	0	0
3	3	[A1,A2,A3]	3	3	B	3	3	C	3	3	D	3	3	E	3	3	F	3	3	0	0	0

Table 7. Configurations and total thickness

	Crystal Thickness (mm)												
	0.17	0.15	0.14	0.13	0.12	0.11	0.1	0.09	0.08	0.07	0.06	0.05	Total thickness at each position
Configuration													
3 (14 off)							42						0.1
A1						1		1					0.2
A2					1				1				0.2
A3					1				1				0.2
B1						4							0.44
B2						4							0.44
B3						4							0.44
C1					5								0.6
C2					5								0.6
C3					5								0.6
D1					6								0.72
D2					1			4	3				0.72
D3					3	1		1	2				0.72
E1						1		9	1				1
E2				6	1		1						1
E3				1		1			5	2	2	2	1
F1			3	6									1.2
F2			8						1				1.2
F3	2	5					1						1.19

muscovite mica analyser bank and the standard polyethylene sample was used for inter-detector calibration purposes. Figure 10 shows the integrated intensity as a function of the detector angle, 2θ, after this correction has been applied. Note that the detectors have been grouped in two's to improve statistics. The line is a guide to the eye.

It is clear that the thickness variation on the analyser bank is reflected in the detected neutron flux. The drop-off at the highest angles occurs because there are no crystals on the analyser support past 2θ =150° and the quite coarse angular resolution of the instrument means that detectors at angles just below 150° are affected as well.

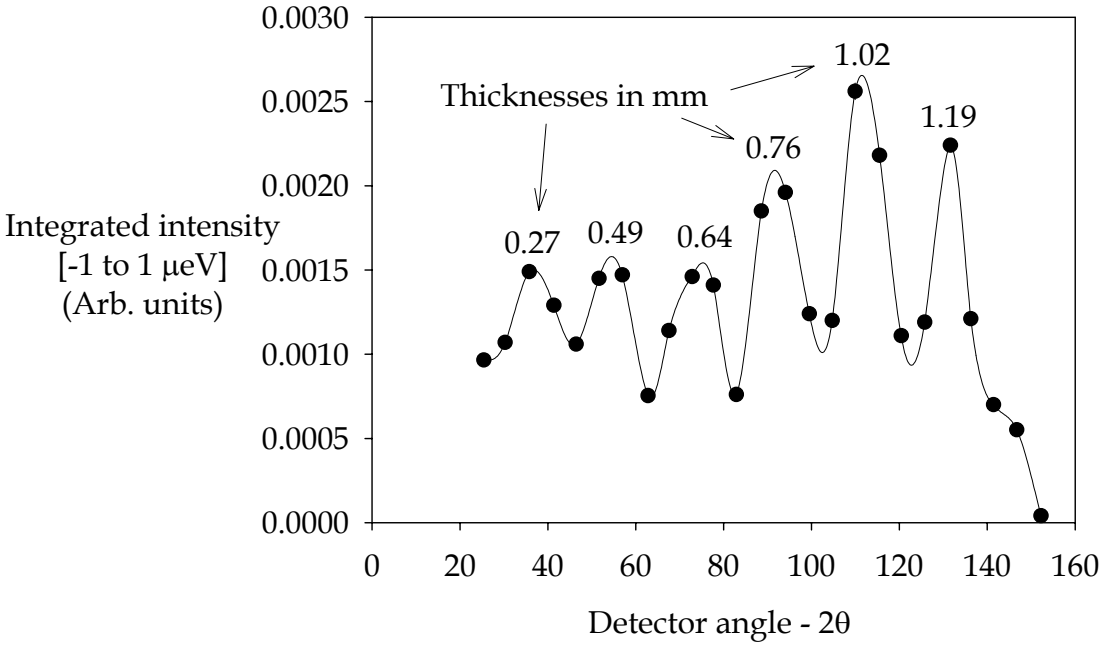

Figure 10. Integrated intensity [-1 to 1 μeV] as a function of detector angle

The spectra at selected 2θ-values (corresponding roughly to the peaks in the above figure) were fitted by Gaussians in order to ascertain the effect of thickness on the resolution function and signal-background. The variation in resolution as a function of 2θ is shown in Table 8. Unfortunately the statistical quality of the data was too poor to extract the signal-background level using this method.

Table 8. Fitted Gaussian parameters for varying thickness of fluorophlogopite

2θ (degrees)	35.8	57.0	72.9	94.0	109.9	131.6
Average thickness (mm)	0.27	0.49	0.64	0.76	1.02	1.19
Amplitude	1.4523	1.4192	1.3638	1.6716	2.1271	1.8513
FWHM (μeV)	0.98	0.99	1.02	1.15	1.19	1.2

This shows that the intensity does increase with thickness and, more importantly, that the maximum in intensity has not been reached. In addition, however, the resolution degrades with thickness. It is very likely that this is as a result of a broadened mosaic spread introduced by stacking crystals together. This would also account for some of the increase in intensity. The results are promising but inconclusive and so further measurements were carried out on the MORPHEUS diffractometer at the Paul Scherrer Institute in Switzerland.

MORPHEUS

MORPHEUS is a versatile 2-axis diffractometer at the SINQ neutron scattering facility located at the Paul Scherrer Institute in Switzerland on, what used to be called, the TOPSI beamline. It is used for amongst other things, single crystal diffraction measurements. It uses neutrons from the liquid D_2 cold source with a peak flux at 4Å. These neutrons are transported along an m=2 Ni-Ti supermirror guide to the monochromator housing where there is a vertically focussing monochromator which consists of a grid of crystals of highly oriented pyrolytic graphite (PG) joined to silicon crystals which have been cut so that there is a 7.22° mismatch between the Si-(111) planes and the (00*l*) planes of the graphite. This gives the possibility of selecting different reflections.

For single crystal experiments a variety of sample manipulation tables are available: sample ω-rotation (-170° to 188° [± 0.002°]); detector arm 2θ-rotation (-125° to +130° [± 0.002°]); sample x and y translation stages (± 18 mm) and sample x and y tilt stages (± 20°). It is also possible to install an Euler cradle.

For this experiment the PG (002) reflection was chosen (d_{200} = 3.3504Å) and the monochromator angle was set to provide neutrons with a wavelength of 5.192458 Å. The experimental setup is shown in figures 11 and 12.

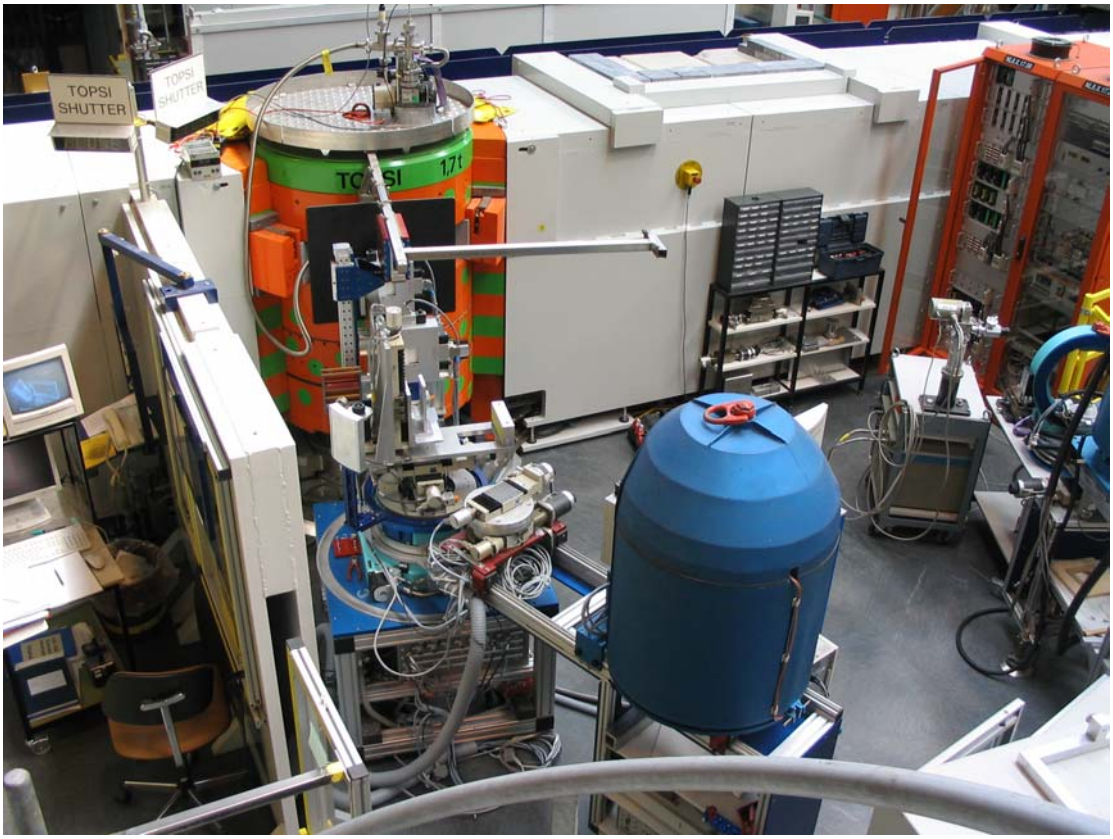

Figure 11. View from above of MORPHEUS experimental setup

Figure 12. Side view of MORPHEUS experimental setup

For this experiment the mica crystals were supported on a cadmium-covered aluminium alloy plate held on a yoke assembly which allowed the sample to be rotated around the vertical axis and moved laterally in all three orthogonal directions (fig. 13). In addition to the cadmium-covered screw in the centre of the crystal note that the bottom of the crystal had to be forced flat to ensure that it followed the profile of the mounting plate. The size of the

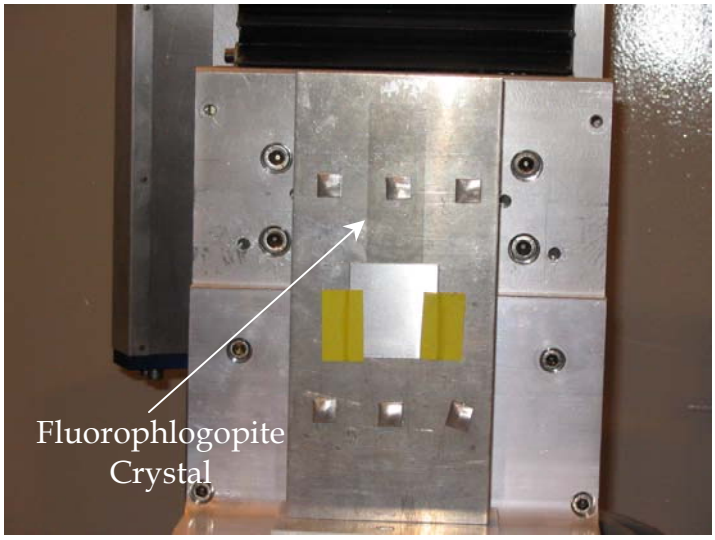

Figure 13. Mounting plate plus mica crystal

incident beam was defined by adjustable apertures to be nominally 1cm high and 1mm wide. The crystals were positioned such that the beam illuminated an area mid-way between the cadmium covered attachment screw and the bottom of the crystals.

Comparison of muscovite and fluorophlogopite

Before discussing the effect of varying the thickness of the fluorophlogopite we show a comparison that was made between fluorophlogopite and muscovite in a θ-2θ scan. The (002), (004) and (006) reflections for both materials (two thicknesses for the fluorophlogopite) are shown in figure 14. There are two things of note. Firstly, the (004) reflection in fluorophlogopite is much weaker than in muscovite. Assuming the intensity of the fluorophlogopite scales linearly up to 0.25mm, which from the IRIS data is a very reasonable assumption, then for the same thickness as the muscovite a peak height of roughly 1/3 that of the muscovite reflection is expected. Secondly, the reflected intensity from the (002) and (006) reflections are far superior in fluorophlogopite.

The peaks for both of the muscovite and thick fluorophlogopite datasets were fitted with a Gaussian area function of the form:

$$y = \frac{a_0}{\sqrt{2\pi a_2}} \exp\left[-\frac{1}{2}\left(\frac{x - a_1}{a_2} \right)^2 \right] \qquad (4)$$

where a_0 is the area, a_1 is the centre and a_2 is the width (≡ $FWHM/2.35482$). The results of this are shown in Table 9.

Table 9. Fitted parameters for the measured reflections of muscovite and fluorophlogopite

MICA	Reflection	a_0	a_1	$FWHM$
Fluorophlogopite	002	3186.0±37.3	30.00±0.0026	0.08
	004	223.2±40.5	62.16±0.0480	0.10
	006	1260.2±50.7	101.46±0.0160	0.15
Muscovite	002	189.2±1.6	30.01±0.0010	0.04
	004	120.3±2.4	62.24±0.0051	0.10
	006	137.7±3.9	101.55±0.0137	0.48

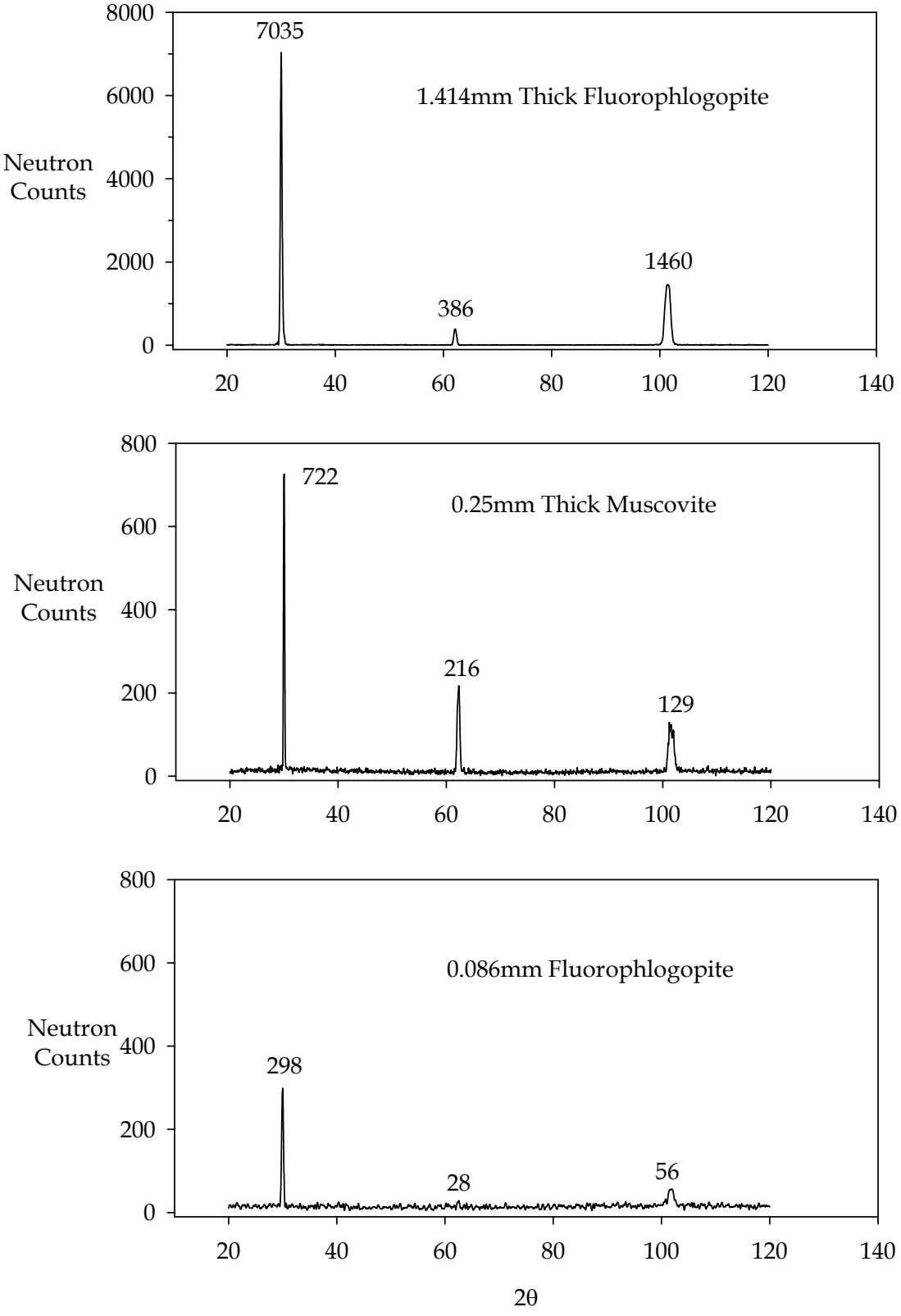

Figure 14. Comparison of muscovite and fluorophlogopite

Effect of thickness on the (002) Reflection of Fluorophlogopite – Part 2

The thickness was varied by stacking crystals together and measuring the thickness obtained using a micrometer. The crystals were then attached to the support plate. A preliminary measurement was then made to check that the resulting Bragg peak was singular and well-defined. At the larger thicknesses this required increasing amounts of clamping pressure and at a thickness of 2.710mm it proved impossible even using the arrangement shown in figure 15 to obtain a singular Bragg peak. It is very likely that this problem is caused by the thinness (and hence flexibility/tendency to bend) of the fluorophlogopite crystals. The muscovite crystals used up until now on IRIS being 0.25mm thick do not suffer from the same problem. Clearly, this is an important issue for any future use of fluorophlogopite on IRIS.

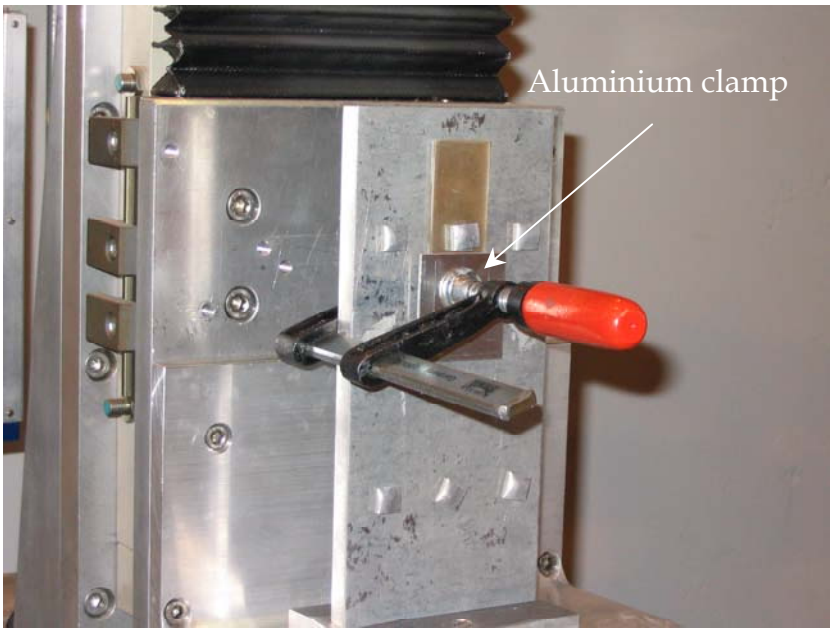

Figure 15. Clamping arrangement for 2.710mm thick fluorophlogopite

The resultant reflected intensity profile for a selection of thicknesses is shown in figure 16. The peaks were again fitted with a Gaussian area function and the integrated peak intensity as a function of thickness is shown in figure 17 along with a fit to the following functional form:

$$y = a\left(1 - e^{-bx}\right) \qquad (3)$$

which is appropriate because the intensity is expected to saturate at a fixed value because of beam attenuation (extinction, absorption and incoherent scattering).

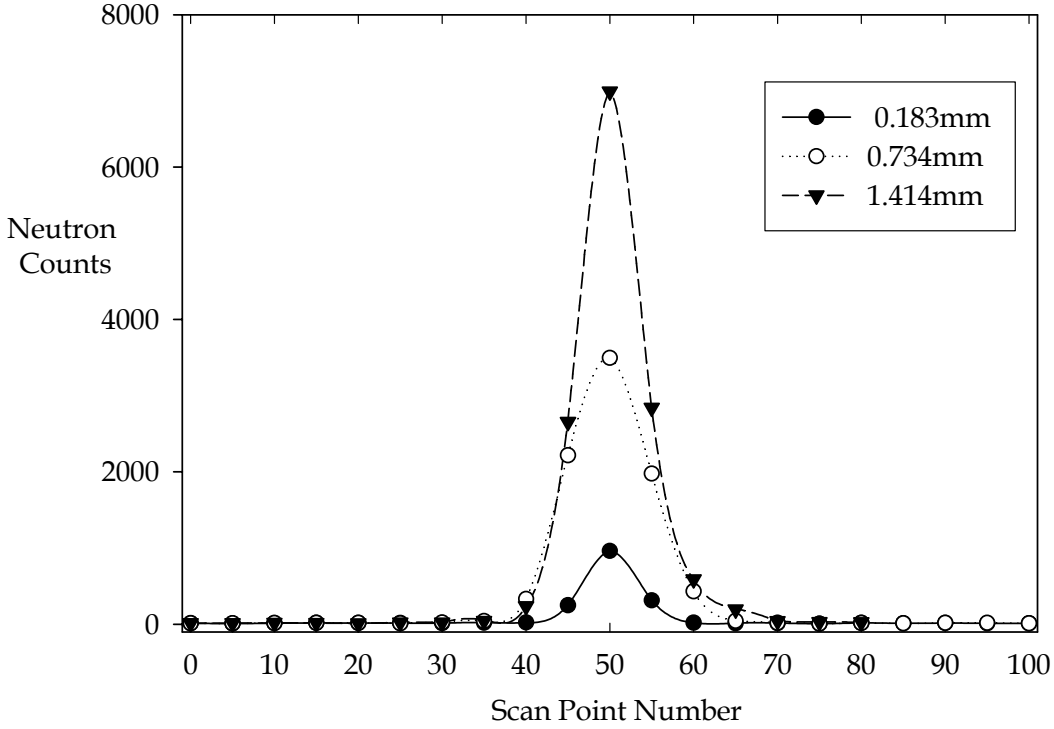

Figure 16. Fluorophlogopite (002) peaks for a selection of thicknesses

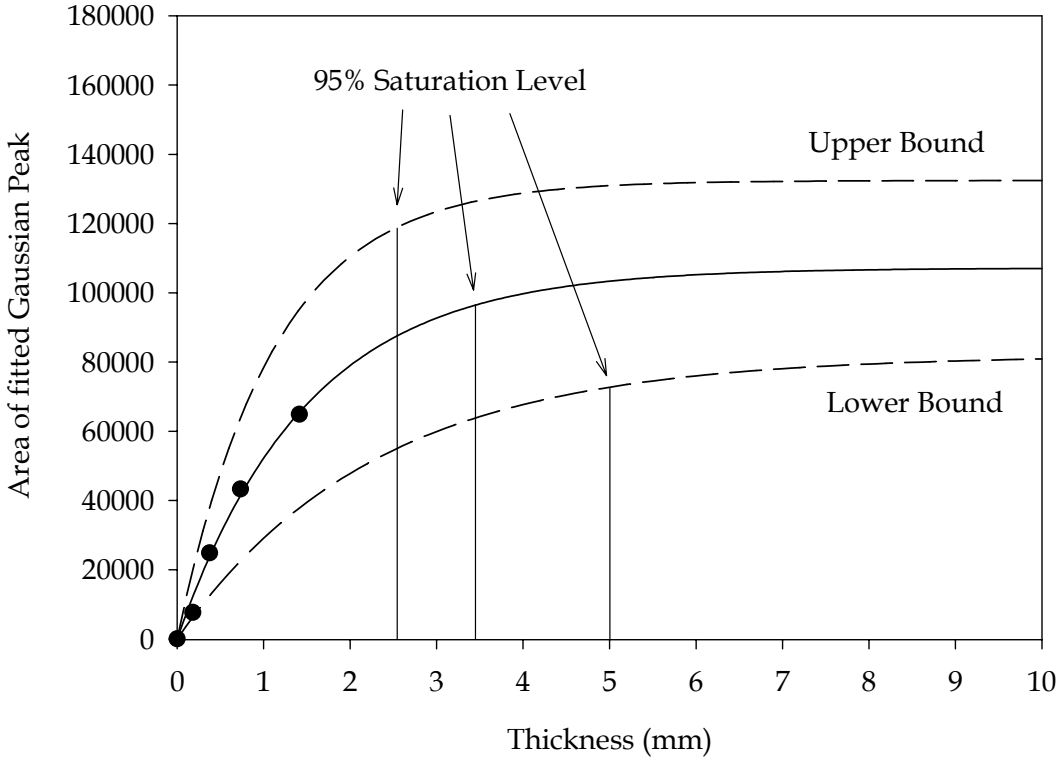

Figure 17. Plot of integrated intensity vs. thickness for fluorophlogopite

In determining the effect of thickness on reflected intensity the scattering angle used during the measurement has to be taken into

consideration. If it is the attenuation due to the incoherent scattering cross-section and the effect of secondary extinction which is important then the total flightpath of the neutrons through the crystals is the governing factor, not the thickness of the crystals per se. At a scattering angle of 15^{o} the distance travelled through the crystals by the neutrons could be considerably larger than the thickness of the crystal stack (see Table 10 below).

Table 10. Thickness of crystal stack and maximum pathlength traversed by a neutron for a scattering angle of 15˚

Measured thickness (mm)	0.183	0.734	1.414
Maximum thickness that the neutrons could possibly be traversing (mm)	1.414	5.672	10.926

Obviously, the average flightpath through the crystal stack is the important factor but this is not a straightforward calculation to make and may best be determined with the use of Monte Carlo simulation. What can be said now however is that if this information can be extrapolated to the case of IRIS with its close-to- backscattering geometry then the potential increase in available intensity is very significant. At a scattering angle of 15^{o} a saturation thickness of 5mm corresponds to a maximum flightpath through the crystals of almost 40mm. This means that on IRIS it should be possible to continue to gain in intensity up to a crystal thickness of 20mm. Given that 0.1mm thick fluorophlogopite is equivalent in intensity terms to 1mm thick of muscovite this equates to a potential intensity gain factor ~200.

Conclusions

Very significant gains in intensity are expected for fluorophlogopite c.f. muscovite mica even for the 'weak' (004) reflection. In particular the (002) reflection could be increased by a factor ~200 making it more intense even than the PG002 reflection.

The improvement in signal-background for the (002) reflection ~ 70% which is significant but nowhere near what is expected from the reduction in incoherent scattering cross-section alone. This implies that there are other sources of background which need to be identified.

Before proceeding with the purchase and installation of large-area analysers of thick fluorinated mica the effect of secondary extinction must be investigated. Experiments to quantify this are planned for IRIS and the ISIS single crystal diffractometer, SXD.

References

1 C. J. Carlile and M. A. Adams, *Physica B* **182,** 431-440 (1992).

2 M. A. Adams, RAL-TR-97-052 (Rutherford Appleton Laboratory, Chilton, 1997).

3 ***Guinness World Records 2004***, edited by S. Newport (Time Inc Home Entertainment, 2003).

4 C. J. Carlile, M. A. Adams, P. R. Krishna, M. Prager, K. Shibata, and P. Westerhuijs, *Nuclear Instruments & Methods In Physics Research Section A-Accelerators Spectrometers Detectors And Associated Equipment* **338,** 78-82 (1994).

5 D. Barthelmy, http://webmineral.com/,(2004) .

6 S. Covey, http://mineral.galleries.com/, (2004).

7 A. R. Lennie, http://www.minweb.co.uk/, (2004).

8 M. Rieder, G. Cavazzini, Y. S. D'Yakonov, V. A. Frank-Kamenetskii, G. Gottardi, S. Guggenheim, P. V. Koval, G. Muller, A. M. R. Neiva, E. W. Radoslovich, J. L. Robert, F. P. Sassi, H. Takeda, Z. Weiss, and D. R. Wones, *Canadian Mineralogist* **36,** 905-912 (1998).

9 M. L. Crow, *Physica B* **241-243,** 110-112 (1998).

10 A. C. Larson and R. B. Von Dreele, GSAS Manual, LAUR 86-748 (Los Alamos National Laboratory, 2000).

Appendix A. Secondary Extinction in Single Crystals

There are two types of secondary extinction. Type I is related to the mosaic spread of the crystal and type II relates to the size of the individual crystallites.

The effect of extinction is to reduce the reflected intensity and this can be described [10] by a scaling factor E_h which is applied to the structure factor in the following way:

$$F_c^{'2} = F_c^2 / E_h$$

In the Gaussian approximation,

$$E_h = \sqrt{1 + 2x + \frac{\left(0.58 + 0.48\cos 2\Theta + 0.24\cos^2 2\Theta\right)x^2}{1 + \left(0.02 - 0.025\cos 2\Theta\right)x}}$$

with 2Θ being the scattering angle. The extinction factor, x, depends upon the type of extinction and the technique being used (x-rays, constant wavelength neutrons and time-of-flight neutrons).

For neutrons the value of x for type II secondary extinction is given by:

$$x = \frac{\lambda^2 F_c^2 \bar{t} E_s}{V_0^2} \times 10^7$$

whereas for type I secondary extinction:

$$x = \frac{\lambda^4 F_c^2 \bar{t} E_g}{V_0^2 \sin^2 \Theta} \times 10^7$$

for time-of-flight neutrons and

$$x = \frac{\lambda^3 F_c^2 \bar{t} E_g}{V_0^2 \sin 2\Theta} \times 10^7$$

for constant wavelength neutrons. In all cases V_0 is the volume of the unit cell and $\bar{t}$ is the mean path through the crystal which must be calculated from considerations of the size, shape and orientation of the crystal. The parameters E_p, E_s and E_g are refineable from experimental data.